Synthesis and Characterization of Chromium Carbide (Cr_3C_2) Nanoparticles

A thesis submitted in partial fulfillment for the
requirement of degree of

Master of Technology
in
Materials and Metallurgical Engineering

by
Shalini Rajpoot
(Roll No. 601102009)

Under the supervision of
Dr. O. P. Pandey
Senior Professor
School of Physics and Materials Science

School of Physics and Materials Science
Thapar University
Patiala-147004, INDIA

July, 2013

"Dedicated to my loving parents"

CERTIFICATE

This is to certify that **Ms. Shalini Rajpoot**, Roll No. 601102009 has worked on this thesis report entitled **"Synthesis and Characterization of Chromium Carbide (Cr_3C_2) Nanoparticles"** as a partial fulfillment for the degree of **Master of technology** in Materials and Metallurgical Engineering. I certify that the matter embodied in this report is of the candidate's own record and not submitted to any other university in any part or full form for the award of such kind of a degree.

O. Pandey 17/7/2013

(Dr. O. P. Pandey)

Supervisor

School of Physics and Materials Science
Thapar University, Patiala

Countersigned by:

Dr. Kulvir Singh
(Professor & Head)
School of Physics and Materials Science
Thapar University, Patiala

Dr. S. K. Mohapatra
Dean of Academic Affairs
Thapar University, Patiala.

ACKNOWLEDGEMENT

First of all, I thank God, the almighty of all who has given me the immense strength and patience to complete my dissertation report in time.

I feel fortunate enough in completing this work under inspiring guidance of ***Dr. O. P. Pandey, Senior Professor, School of Physics and Materials Science****, I express my deep sense of gratitude to him for his incisive comments, fruitful discussions and valuable suggestions that always edify me with enthusiasm to carry out my work firmly.*

I wish to express my sincere thanks to ***Dr. Kulvir Singh, Professor and Head, School of Physics and Materials Science*** *for his constant guidance and encouragement. I am also thankful to* ***Dr. B. N. Chudasama*** *for his effective support and all the faculty members of School of Physics and Materials Science for their constructive suggestions at different stages of this work.*

It gives me immense pleasure to express my special thanks to research scholars ***Ms. Mani Mahajan*** *and* ***Mr. Gourav Singla****, for their keen interest and collaboration during my work.*

Most importantly, I would like to express my heart-felt gratitude to my family. None of this would have been possible without their love and patience.

Last but not the least, I would like to convey my sincere gratitude to ***Mr. Paramjyot Kumar Jha, Mr. Suresh Kumar, Mr. Kapil Sood, Ms. Jagdeep Kour, Ms. Samita Thakur, Mr. Satwinder Danewalia,*** *research scholars of School of Physics and Materials Science, Thapar University,* ***Mr. Vipin Sharma (IITR),*** *my friends and colleagues for their support and their timely help and valuable discussions.*

Shalini Rajput

(SHALINI RAJPOOT)

Abstract

Carbides, a very unique field of research, becoming very attractive and promising candidates in modern scientific and technological applications. Among these, chromium carbide exhibit extremely good strength, hardness, anti-erosion and corrosion properties, surface characteristic, etc. Also, chromium carbide acts as a grain growth inhibitor, widely used in composites by the incorporation of different secondary phase, such as fine grains of cemented carbides WC-Co and Al_2O_3 matrix. Because of these inherent properties chromium carbides are found excellent reinforcement for toughening purpose owing to its high Young's modulus, making it most demanding material among carbides. These properties are further enhanced by synthesizing chromium carbide in nano scale. Nano grained materials exhibit superior properties than conventional one.

The present work is an attempt to synthesize chromium carbide (Cr_3C_2) nanoparticles by thermo-chemical reaction route where chromium oxide (Cr_2O_3) is reduced to nano- chromium carbide (Cr_3C_2) at temperature range 600-800^oC. The phase identification of the product phase(s) was done by X-ray diffraction and Transmission electron microscope techniques.

CONTENTS

LIST OF TABLES

LIST OF FIGURES

LIST OF ABBREVIATIONS

XRD	X-ray diffraction
TEM	Transmission electron microscopy
SADP	Selected area diffraction pattern
EDS	Energy dispersive spectroscopy
Cr_3C_2	Chromium carbide
CNS	Carbon nanospheres
CNTs	Carbon nanotubes

CHAPTER 1

INTRODUCTION

1.1 General information on carbides

Transition metal carbides are the materials exhibiting numerous industrial applications with promising future for scientific community. Although most of their applications are recent though the refractory carbides have been known for over one hundred years. Because of their high melting point, high hardness, high temperature strength, high Young's modulus, high anti wear properties, they are used in cutting tools, dies, abrasives, as anti-wear coating. Moreover, their performance under severe temperature gradients, along with thermal shock, fatigue, abrasion, attrition and chemically induced wear is better [1, 2]. Apart from these properties, the transition metal carbides have large potential to replace Pt/Pd in heterogeneous catalysis also [3]. Due to the attractive properties of these metal carbides, they are becoming promising candidates for the modern industry in a very short time.

1.2 Refractory Carbides

Transition metal forming carbides in Groups IV-VI have very high melting points and are therefore referred to collectively as “refractory carbides”. The term refractory means a material with high melting point, arbitrarily fixed at >1800^{o}C, as well as high degree of chemical stability. The intermediate and salt-like carbides do not fulfil one or both of these qualifications and therefore, cannot be considered as refractory. Only the interstitial and covalent carbides fulfil these conditions [4].

1.3 Classification

The refractory carbides, their classification and general features are categorized on the basis of structural characteristics. These materials can be divided into two major types:

- The interstitial carbides (formed by element of Box A).
- The covalent carbides (formed by element of Box B).

Table 1.1 Periodic table of the elements showing their electro-negativity and elements forming the refractory carbides [4].

H																
2.1											BOX B					
Li	Be										B	C	N	O	F	
1.9	1.5										2.0	2.5	3.0	3.5	4.0	
Na	Mg										Al	Si	P	S	Cl	
0.9	1.2		BOX A								1.5	1.8	2.1	2.5	3.0	
K	Ca	Sc	Ti	V	Cr	Mn	Fe	Co	Ni	Cu	Zn	Ga	Ge	As	Se	Br
0.9	1.0	1.3	1.5	1.6	1.6	1.5	1.8	1.8	1.8	1.0	1.6	1.6	1.8	2.0	2.4	2.8
Rb	Sr	Y	Zr	Nb	Mo	Te	Ru	Rh	Pd	Ag	Cd	In	Sn	Sb	Te	I
0.8	1.0	1.2	1.4	1.6	1.8	1.9	2.2	2.2	2.2	1.9	1.7	1.7	1.8	1.9	2.1	2.5
Ca	Ba	La	Hf	Ta	W	Re	Os	Ir	Pt	Au	Hg	Tl	Pb	Bi	Po	At
0.7	0.9	1.1	1.3	1.5	1.7	1.9	2.2	2.2	2.2	2.4	1.9	1.8	1.8	1.9	2.0	2.2

1.4 Factors controlling carbide formation

There are three general factors which play vital role in the formation of carbides, i.e. the difference in electro-negativity between carbon and the other elements, the size of the respective atoms and the bonding characteristics of these atoms. These factors are examined in the following three sections:

1.4.1 Electronegativity

The difference in electro-negativity between carbon and other elements forming carbides is an important factor in determining the nature of the compound. As shown in the table 1.1, the difference in the interstitial carbides is large (Box A) while it is much less pronounced in the covalent carbides (Box B).

1.4.2 Atomic radii

The atomic radius of the constituent elements is the second factor controlling carbide formation. If the difference of atomic radius between carbon and other elements forming a carbide is large, interstitial carbides are formed (e.g., Cr_3C_2) and for the covalent carbides formation, this difference is small (e.g., SiC) [5]. Atomic radii of some elements are shown in table 1.2.

Table 1.2 Approximate atomic radius of carbon and selected elements [5].

Element	Atomic Number	Atomic Radius (nm)
Boron	**5**	**0.088**
CARBON	**6**	**0.078**
Nitrogen	**7**	**0.074**
Oxygen	**8**	**0.066**
Aluminum	**13**	**0.126**
Silicon	**14**	**0.117**
Titanium	**22**	**0.1467**
Vanadium	**23**	**0.1338**
Chromium	**24**	**0.1267**
Manganese	**25**	**0.1261**
Iron	**26**	**0.1260**
Cobalt	**27**	**0.1252**
Nickel	**28**	**0.1244**
Zirconium	**40**	**0.1597**
Niobium	**41**	**0.1456**
Molybdenum	**42**	**0.1386**
Hafnium	**72**	**0.1585**
Tantalum	**73**	**0.1457**
Tungsten	**74**	**0.1394**

1.4.3 Bonding properties of carbides

Interstitial carbides

The difference in electro-negativity between the two elements of the interstitial carbides is large. They are so called interstitial because the carbon atom has a much smaller size than the other atoms, allowing it to nest in the interstices of the lattice. For the formation of an interstitial structure, the ratio of the radius of the interstitial atom to the radius of the atom of the host metal must be less than 0.59. The bonding is partly covalent and ionic, but mostly metallic which explains why the interstitial carbides closely resemble metals. Like metallic alloys, their electrical and thermal conductivities are high. In addition, they have high melting points, high hardness and are chemically inert and fully qualify the ‘‘refractory criteria’’ [6].

Covalent carbides

The difference in electro-negativity between the two elements of the covalent carbides is small. Since the carbon atom is slightly smaller than the other atom so they form covalent bond. Only two covalent carbides, silicon carbide and boron carbide, fully meet the refractory criteria. Other carbides such as Be_2C, are only partially covalent while they have high melting point but are generally not chemically stable and are therefore, not considered here.

1.5 Classification on the basis of group of elements

1.5.1 Group IV carbides (Ti, Zr, and Hf carbides)

This section shows the characteristics of the interstitial carbides formed by the metals of group IV: Titanium, Zirconium and Hafnium. The rationale for reviewing this compound together in one chapter is their similarity in atomic bonding, composition and crystallography which is summarized as follows:

i. The metal-to-metal bond is relatively weak and the metal-to-carbon bond is strong.

ii. The only stable composition is the monocarbide with carbon atoms in all octahedral sites.

iii. The major crystalline structure is CCP with FCC symmetry (NaCl).

1.5.2 Group V carbides (V, Nb and Ta carbides)

This section shows the characteristics of the interstitial carbides formed by the metals of group V: Vanadium, Niobium, and Tantalum. These three carbides have similar atomic bonding, composition and crystallography and are summarized below:

i. Both metal-to-metal and metal-to-carbon bonds are strong.

ii. Unlike the carbides of group IV, they have two compositions:

- a subcarbide, M_2C with carbon atoms in half of the octahedral sites.
- a monocarbide, MC with carbon atoms in all octahedral sites (at stoichiometry).

iii. They have two crystalline structures: HCP (M_2C) and CCP (MC) with FCC symmetry (NaCl).

1.5.3 Group VI carbides (Cr, Mo, and W carbides)

This section shows the characteristics of the interstitial carbides formed by the metals of group VI: Chromium, Molybdenum and Tungsten. These three carbides have similar atomic bonding, composition and crystallography. They have a more complex composition and crystallography than the carbides of group IV and V. They have several compositions as [7]:

$Cr_{23}C_6$, Mo_2C, W_2C,

Cr_7C_3, Mo_3C_2, WC,

Cr_3C_2

Their structural characteristics can be summarized as follows:

i. They have two major crystalline structures: Hexagonal and Orthorhombic.

ii. The mono carbide form is retained in MoC and WC but, unlike the carbon atoms in MoC

and WC occupy the more spacious trigonal prismatic sites (hexagonal structure) [8, 9].

iii. The metal-to-metal bonds are strong and the metal-to-carbon bonds are weak.

iv. The carbides of group VI are important industrial materials, particularly tungsten carbide and chromium carbide.

1.6 Nano materials

Miniaturization is a general aim of the technology that is taking place to produce smaller, faster, lighter and cheaper materials with greater performance while using fewer raw materials. Research on nano materials is a step towards miniaturization of technology that will contribute significantly towards a sustainable usage of raw materials and energy. Properties of nano particles are different and often superior to their conventional counterparts having polycrystalline structure. These properties depend on the microstructure which is determined by the chemical composition, grain size, atomic structure, crystallographic orientation and dimensionality. Nano particles, due to their smaller size and a large surface to volume ratio, exhibit interesting novel properties which include nonlinear optical behaviour, increased mechanical strength, enhanced diffusivity, high specific heat, magnetic behaviour and electric resistivity etc.

The unique properties of nano-sized particles and nano grain bulk materials can be attributed to two basic phenomena. The first is that the number of atoms at the surface and/or grain boundaries in these materials is comparable to that of the atoms located in the crystal lattice, thus the chemical and physical properties are increasingly dominated by the atoms at these locations. The second phenomenon is the “quantum size effect” or “quantum confinement effect”. When particles approach the nanometer scale range, their photonic and electronic properties can be significantly modified as a result of the absence of a few atoms in the lattice and the resulting relaxation of the lattice structure.

Moreover, for processing of advanced ceramics the particle size of the starting powder is an important parameter. Small size particle provides ductility through differential creep mechanisms and allow for greater densification because of the dependence of sintering on the inverse fourth power of particle size. Fine and uniform distribution of carbides in ductile metal matrix can give excellent results like longer tool life. By reducing the size from micro to nano, these materials show different properties because of the high surface to volume ratio. This is the reason that the interest in synthesis of high surface area materials has grown in recent years. Nano carbides have the potential to become the new materials for tools, dies and wear parts.

1.7 Chromium carbide properties and applications

Among the transition metal carbides, chromium carbide (Cr_3C_2) is a hard refractory ceramic that exhibits excellent strength, hardness, anti-erosion and corrosion properties, permanent non-magnetizability and surface characteristics [22]. Therefore, chromium carbides have been widely used in a variety of industrial applications, such as shaft bearings, seals, high-temperature furnaces, nozzles and metal machining molds [23]. It is usually processed by sintering. It has the appearance of grey powder with orthorhombic crystal structure in which the host-metal atoms are generally arranged in a close-packed structure and the carbon occupies specific interstitial sites in that structure [4]. Chromium carbides (CrC_x) consist of three crystallographic structures such as cubic $Cr_{23}C_6$, hexagonal Cr_7C_3 and orthorhombic Cr_3C_2. Among them, the orthorhombic Cr_3C_2 occurs extremely rare as mineral tongbaite. It is highly corrosion-resistant and does not oxidize even at high temperature (1000-1100°C) [14].

It is well known that alumina is one of most important material in structural ceramic application because of its tremendous physical, thermal and chemical properties. Its intrinsic brittleness and relatively poor reliability however, made the toughening of alumina ceramics as an important

and challenging area of research now days. The aim of the composites is to improve the mechanical properties such as hardness, facture strength, toughness and also high temperature mechanical properties such as hardness, strength, creep and fatigue facture resistances. There are several approaches by the researchers to toughen the alumina matrix by the incorporation of different secondary phases. Among all the approaches, chromium carbides are found to be excellent reinforcement for toughening purpose owing to its high Young's modulus and its high temperature erosion resistance.

Alumina-chromium carbide composites are well known for their good mechanical properties in comparison with pure alumina or metals. It can be observed that the nanocomposite exhibits improved hardness, fracture strength and facture toughness in comparison to monolithic alumina [24]. The mechanical properties of monolithic Al_2O_3 and Cr_3C_2/Al_2O_3 nanocomposites are shown in the table 1.3.

Table 1.3 Mechanical property of monolithic Al_2O_3 and Cr_3C_2/Al_2O_3 nanocomposites [24].

Material	**Hardness GPa**	**Strength (4-point blending) MPa**	**Toughness (Indentation Fracture method) MPa. m½**
Al_2O_3	**18.4**	**375**	**4.0**
Cr_3C_2/Al_2O_3	**19.8**	**520**	**5.5**

Chromium carbide (Cr_3C_2) as grain growth inhibitor

Cermets WC-Co are widely known material for their high wear resistance which are used in various applications such as metal cutting and rock drilling tools and wear parts. Cermets which are composed of carbo nitride based materials such as TiCN, on the other hand are more wear resistant than cemented carbides, but may not be as tough. It is well known that nano sized grain and sub-micron WC-Co composites have superior properties than those of the conventional WC-Co composites. One method to decrease the grain size by using special alloying elements called grain growth inhibitors. Grain growth inhibitors are used to palliate grain growth during sintering. Refractory carbides mainly vanadium carbide (VC) and chromium carbide (Cr_3C_2) are by far the most effective grain growth inhibitors and are widely practiced in the industry for sintering ultrafine WC-Co composite due to their high solubility and mobility in cobalt phase at lower temperatures [25]. In addition, the combinations of VC and Cr_3C_2 shows better inhibition effects than that of single one doped [26].

The effectiveness of transition metal carbides as grain growth inhibitor is related to its thermodynamic stability and they are ranked as follows [27]:

$$VC > Mo_2C > Cr_3C_2 > NbC > TaC > TiC > Zr/HfC$$

It was also found that there is a maximum level above which no further grain growth inhibitor works. This level corresponds to the maximum solubility of the carbide phase in liquid cobalt. A liquid phase that is saturated with inhibitor carbide would reduce the solubility of WC and thereby reduce its coarsening rate [27]. Some properties of refractory carbides and binder materials are shown in table 1.4.

Table 1.4 Properties of refractory carbides and binder materials [27].

Material	**Hardness HV (50 Kg)**	**Modulus of elasticity, GPa**	**Melting temperature, ^{o}C**	**Theoretical density, gm/cc**	**Thermal expansion, µm/m.K**
WC	2200	696	2800	15.63	5.2
W_2C	3000	-	2777	17.3	-
TiC	3000	451	3100	4.94	7.7
VC	2900	422	2700	5.71	7.2
HfC	2600	352	3900	12.76	6.6
ZrC	2700	348	3400	6.56	6.7
NbC	2000	338	3600	7.8	6.7
TaC	1800	285	3800	14.50	6.3
Cr_3C_2	1400	373	1800	6.66	10.3
Co	< 100	207	1495	8.9	16
Ni	<100	207	1455	8.9	15

1.8 Origin of problem

Interstitial transition metal compounds can be formed by the consolidation of carbon and nitrogen into the lattices of transition metals to produce a higher class of compounds with exclusive physical and mechanical properties.

The applications of the interstitial compounds take advantage of this fact that they are hard, high melting point and have a metallic character [10]. In many cases, their catalytic properties are also durable and similar with the group VIII metals [11]. The group VI metals (chromium, molybdenum, tungsten) come at border line position; Mo and W carbides show simple structures as in group IV and V but the chromium carbides have more complex structures [12]. In case of chromium, Hagg's rule shows that if the metal atoms are smaller than the other (carbon), the metal lattice undergoes a major distortion when carbon atom is incorporated. The chromium carbide (Cr_3C_2) has direct C-C bonds that form chains. As M-C bonds decrease with increasing C-C bonds, the system evolves into graphite by the way of a sequence of metastable states as in the case of iron, nickel etc. [13] . Since they are refractory in nature, they are widely used in corrosive environments as wear resistant and protective coatings. Moreover, they are also used for conventional coatings such as electrochemical hard chrome in mold protection [14]. The low surface energy of the coating can also simplify the mold releasing operation of injected parts.

Chromium carbides as crystalline powder are used as reinforcement agents for composite materials and cermets both in bulk form and in thick film coatings deposited by thermal spray technique [15]. Moreover, these properties are further enhanced if processed in nano scale.

In recent years, many synthesis techniques have been proposed to prepare materials having particles of nanometer-size such as physical vapour deposition (PVD) [16], metal atom vaporization [17], chemical vapor deposition (CVD), reactive evaporation and sputtering [18], liquid-phase methods including, sol-gel chemistry [19], gas reduction-carburization [20], and mechanical-thermal synthesis [21]. But all of these techniques are high temperature and produce low yield. Considering these facts, the present study is planned to synthesize Cr_3C_2 at low temperature to reduce its production cost.

CHAPTER 2

LITERATURE REVIEW

The invention of the carbide tool materials was first disclosed in 1923 in Karl Schrter's patent application [28]. Then the findings by Schwarzkopf showed that solid solutions of carbides are superior to individual carbide which was the starting point of the development of multi-carbide cutting tools for high-speed machining of steel [29].

Carburization of metastable chromium dioxide (CrO_2) and chromium (III) oxide (Cr_2O_3) in methane-containing gas mixture, such as CH_4–H_2–Ar and CH_4–H_2, can also lead to chromium carbide formation [30, 31].

The most important advancement in cutting tool technology was the development of coated tools in seventies [32, 33]. Coatings are the diffusion barriers and they prevent the interaction between the chips formed during machining and the cutting materials. The synthesis of nano structured Cr-C started in 1992 [34].

Ivanov *et al.* [34] synthesized chromium carbide by mechanical alloying of Cr and C at low temperature. It has been found that using high energy milling, all starting material can be transformed directly into one phase as final product. The main drawback of mechanical alloying was long milling time required to refine the powders. This makes the efficiency low and induces contamination from milling media and atmosphere.

Lerch *et al.* [35] reported that the $CrO_{1.9}$ with high surface area (200–350 m^2/g) reduced at 700°C in an atmosphere of methane and hydrogen mixture leading to the formation of stable Cr_3C_2 and metastable Cr_3C_{2-x}. The metastable Cr_3C_{2-x} powder was also prepared by **Loubiere *et al.* [36, 37]** using CH_4–H_2 atmosphere from the carburization of metastable chromium oxide.

Walter *et al.* [38] used plasma source ion implantation (PSII) processes using three gases i.e. either ammonia (NH_3), methane (CH_4), or oxygen (O_2) to increase wear resistance of electro-deposited chromium. Their results indicate the formation of hard compounds, namely polycrystalline chromium-nitride (CrN) w.r.t. ammonia (NH_3), chromium-carbide (Cr_3C_2) w.r.t. methane (CH_4), and chromium-oxide (Cr_2O_3) w.r.t. oxygen (O_2). They showed that with the indentation depth (~25 nm or ~50% of the implantation depth), NH_3 implantation increased the surface hardness by 24%. At a similar depth, CH_4 implantation increased the surface hardness by 4% and oxygen implantation increased the hardness by 20%. They also reported that the hardness of the ion implanted surfaces decreased with increasing depth which reflects the decreasing implanted species concentration.

The synthesis of porous chromium carbide through reactive reaction has been reported by **Hashimoto *et al.* [39].** They obtained a mixture of porous chromium carbide, magnesia and chromium oxide by heating the mixture of $MgCr_2O_4$ and graphite powders at 1400–1650^oC for 2h. Chromium carbide was also reported to be formed from the mixtures of chromium oxide, magnesium and carbon by the self propagating high temperature synthesis (SHS) process **[40]**.

Detroye *et al.* [41] presented the synthesis and the characterization of various chromium carbide compounds. In their work, thin $Cr_{23}C_6$ films were deposited by reactive sputtering while Cr_7C_3 films were formed by the carburization of chromium films in a CH_4/H_2 atmosphere. Cr_xC_y powders were synthesized from various precursors (Cr, CrN, Cr_2O_3) by reaction with CH_4/H_2 at temperature (870-1230K) and characterized samples using characterization techniques AES, XRD and electron diffraction.

Preiss *et al.* [42] used vanadium and chromium tartrate precursors prepared from aqueous solutions as pre-ceramic materials for carbothermal reactions with and without simultaneous

nitridation. The carbothermal reactions leading either to V_8C_7, V(C, N, O) solid solution and Cr_3C_2 respectively, proceeded at moderate temperatures between 800 and 1100^oC. But with extensive heat treatment the particles grow and the surface area diminish.

He *et al.* [43] synthesized pre-alloyed Cr_3C_2-25 (Ni20Cr) nanopowder by mechanical ball milling in Hexane [$H_3C(CH_2)_4CH_3$]. They found that initially the average powder size decreased drastically with time during the first four hours of milling, after that the decrement was slow as milling continued up to 20 h. For milling times in excess of four hours, the particle size approached 5 microns and reported that the milling times of up to 20 h led to the formation of a polycrystal nanocomposite powder system in which chromium carbides, with average size of 15nm, were uniformly distributed in NiCr matrix.

Wolfe *et al.* [44] synthesized titanium carbide/chromium carbide multilayer coatings with varying individual layer thicknesses by the co-evaporation of titanium, chromium and carbon (through tungsten) ingots using electron beam-physical vapor deposition. The adhesion of the multilayer coatings was found to be greater than 50 N. They found the hardness of the titanium carbide/ chromium carbide multilayer coatings to increase from 1302 $VHN_{0.050}$ to 2052 $VHN_{0.050}$ by decreasing the thickness of the individual layer from 1.2 to 0.1μm. Also, the average grain diameter was found to decrease from 3.315 to 0.356μm by decreasing the thickness of the individual layers. In addition, they reported the fracture toughness of the TiC/CrC multilayer coatings decreased from 4.179 to 1.411 MPa-$m^{1/2}$ with decreasing layer thickness.

The major aims of the work of **Romero *et al.* [45]** was to obtain Cr/CrC multi-layers with bilayer period thickness in the 300–20 nm range with total coating thickness approximately 1.5 μm onto steel and silicon substrates by alternatively changing the sputtering gas composition between pure argon and a reactive mixture Ar/CH_4.

Su *et al.* [46] investigated the tribological properties of $Cr_{x\%}C$-coated disks and the cutting performance of $Cr_{x\%}C$-coated cemented carbide tools. Experimental results indicate that the coating microstructures, mechanical properties and wear resistance vary according to the chromium content.

Anacleto *et al.* [47] examined reduction of chromium oxide (Cr_2O_3) to chromium carbide (Cr_3C_2) in a bed laboratory reactor in the temperature range 900°C to 1200°C in presence of the mixture of CH_4-H_2-Ar with the addition of CO as the reducing gas. They determined the extent and rate of reduction as function of gas composition and temperature by on-line off-gas analysis using a mass spectrometer.

Teng *et al*. [48] obtained Gibb's energy ($\Delta_f G^o$) of formation for Cr_3C_2 that was -58,857 J/mol and entropy -22.344TJ.mol^{-1}.K^{-1} with total uncertaintity ±1600 J/mol from electromotive force (EMF) measurement, in the temperature range 950 to 1150K, using the galvanic cells with CaF_2 single crystals as the electrolyte: Cr, CrF_2 |CaF_2| CrF_2, Cr_3C_2, C. They also obtained an average value of enthalpy ($\Delta_f H°$) for Cr_3C_2 was -71.7 kJ/mol.

Sen [49] studied the kinetics of chromium carbide-coated high-chromium steel by thermo-reactive diffusion technique. He found that the activation energy for the process was 278 kJ/mol.

Lin *et al*. [50] prepared nano-sized Cr-species particles with a size scale 20–40 nm, which were uniformly coated on alumina particles by metal organic chemical vapor deposition (MOCVD) in the fluidized chamber using the pyrolysis of $Cr(CO)_6$ precursor. In a graphite furnace, carbothermal reactions of Cr-species in an Ar atmosphere at temperature 1250^{o}C for 2h as well as the microstructure of high pressure sintering specimen were reported. After characterizing the deposited powder through an X-ray diffractometer and transmission electron microscopy, they analyzed that the deposited powders were metastable CrC_{1-x} and Cr_2O_3. Thermal treatment as

well as high pressure sintering revealed that Cr-species were transferred into stable chromium carbide (Cr_3C_2 and Cr_7C_3). From the microstructure of sintering specimen, they showed that the cluster of coated nano-particles was formed in the fluidized bed which coarsen during densification and generally were located on the grain boundary to inhibit the alumina grain growth.

Lin *et al.* [51] synthesized chromium carbide films from a Cr target (99.95%) and C_2H_2/Ar gases that varied with two deposition parameters (deposition temperature and substrate bias voltage) using a 90^o bend filtered cathodic vacuum arc (FCVA) system. They found that as the deposition temperature increases from 300 to 500^oC. The morphology of the growing film becomes denser and the microstructure becomes more compact and also analyzed that the film cannot be easily deposited at ambient temperature (without heating) because the coating adhesion is weak and also the compressive stress increases.

Osvaldo *et al.* [52] proposed a mechanical-thermal method to enhance the reaction between Cr and C, which was carried out via high energy milling of the mixtures of metallic chromium and carbon (graphite) and subsequent heat-treatment in an inert atmosphere.

Giordano *et al.* [53] produced a series of nanoparticles of metal nitrides and metal carbides, TiN, VN, NbN, GaN, Mo_2N, W_2N, CrN, NbC(N), TiC(N), WC, Mo_2C, and Cr_3C_2 with the size range 3-30 nm except GaN (with an average size of 50-100nm) at relatively low temperature (800^oC) using simple and mainly nontoxic precursor, i.e. using urea or its close derivatives as both nitrogen or carbon source are the growth controlling system.

As per literature, **Kumar *et al.* [54]** have first performed the experiment under high pressure in a self-designed autoclave to synthesize WC-nanoparticles from WO_3 by thermo-chemical reaction

route. They also reported that this method can be carried out to find a higher yield having uniform and ultrafine particles because of high pressure generated inside the autoclave.

Wang *et al.* [55] have synthesized nano-sized chromium carbide by metal-organic chemical vapor deposition method in a fluidized bed using mixtures of CH_4/H_2 at ambient temperature as carburization source in the temperature range of 700–850°C. They found that the carburization process involved the sequential deposition of carbon on the outer surface of the Cr_2O_3 powder followed by carbon diffusion into the powder, leading to the formation of metastable Cr_3C_{2-x} phase and stable Cr_3C_2. **Kahrizsangi *et al.* [56]** formed chromium carbide by reduction of chromium oxide in 30%-methane gas mixture at 1000°C.

Gomari *et al.* [57] fabricated nanostructure chromium carbides with elemental powders of chromium (150µm, 99% purity) and carbon (100µm, 99% purity) by mechanical alloying in a Fritsch planetary ball mill and the crystallite size of chromium carbides was found to be about 21 nm after 12 h of milling.

Xing *et al.* [58] synthesized porous chromium carbide structure through reactive sintering of chromium oxides in carbonaceous reducing environments (carburization process). They performed carburization at 1000^oC, 1100^oC, 1200^oC and 1300^oC respectively, for 10 h in a reducing atmosphere containing 2% methane and 98% hydrogen.

Zhao *et al.* [59] used the solution-derived precursor method to synthesize chromium carbide (Cr_3C_2) nano-powders by the carburization at lower temperature where ammonium dichromate ($(NH_4)_2Cr_2O_7$) and nanometer carbon black were used as raw materials.

Richert *et al.* [60] studied the properties of nanostructured Cr_3C_2-NiCr coatings, deposited by high velocity oxy-fuel (HVOF) and thermal spraying processes. They investigated that the microhardnes vary with the deposited coatings, such as microhardness was 665 using Cr_3C_2-

NiCr-Plasma spraying, 790 for Cr_3C_2-NiCr- Plasma spraying with propane - butane shield, 863 for Cr_3C_2-NiCr- HVOF and 950 for Cr_3C_2-NiCr +5%E(Ni17Cr4Fe4Si3.5B1C)- Plasma spraying with propane-butane shield. They concluded that introduction of Cr_3C_2NiCr +5%E(Ni17Cr4Fe4Si3.5B1C) - plasma spraying with propane-butane shield in the process of deposition contribute to the better properties of the coatings.

Jiang *et al.* [61] compared chromium carbide (Cr-C) and chromium nitride (Cr-N) powders with a chromium metal powder (Cr-metal) to evaluate their chemical stability in synthetic biological fluids of different pH and composition. They found that higher chromium release was observed from Cr-N compared with Cr-C and studied that it may be related to differences in solubility of CrN and Cr_2N where preferential dissolution of one together with partial dissolution of Cr_2O_3 at lower pH resulted in increased chromium release.

Wang *et al*. [62] synthesized a series of carbides (TiC, V_2C, Mo_2C) from the corresponding metal oxides (TiO_2, V_2O_5, MoO_3), CaC_2 and magnesium as starting materials in a stainless steel autoclave at 600°C. They could also produce transition metal nitrides (TiN, VN and CrN) through similar processes, by employing the corresponding metal oxides (TiO_2, V_2O_5, Cr_2O_3), $NaNH_2$, and magnesium as starting materials at 550 °C.

Mahajan *et al.* [63] synthesized V_8C_7 nanopowders using chemical-reduction route in a self-designed and fabricated autoclave relatively at low temperature at 800°C under high pressure.

Ouyang *et al.* [64] investigated the influence of Cr_3C_2 and VC addition on the microstructure and mechanical properties of WC–MgO composites hot-pressed at 1650°C for 90 min. They found that the grain growth of WC was significantly inhibited and the homogeneity of MgO particulate dispersion was effectively improved with the addition of 0.5 wt.% Cr_3C_2 or 0.5 wt.% VC. They also observed that the load-independent hardness was increased and the indentation

size effect (ISE) on hardness was restrained by doping grain growth inhibitors. Due to the refined WC grains and uniformly dispersed MgO particulates, the improvements on fracture toughness of hot-pressed samples were also observed.

Zheng *et al.* [65] fabricated porous Cr_3C_2 with a continuous open pore structure by a reaction sintering process. They found that as the carbonization temperature increased from 1000 ^oC to 1300 ^oC, the average pore size increased from 0.8 μm to 3.5 μm, while the distribution of the pore diameters became more dispersed. They also reported that as the porosity increased Young's modulus of the porous Cr_3C_2 decreased rapidly and the hardness of the porous Cr_3C_2 is mainly affected by the pore structure and the value of Vickers hardness varied from 20 to 90 as the average pore size increased from 0.8 μm to 3.5 μm.

CHAPTER 3

EXPERIMENTAL

As mentioned in the previous chapter, the basic objective of the present work is to synthesize Cr_3C_2 at low temperature by adopting simple thermo-chemical reaction route. In order to do so the procedure adopted for the preparation of sample and its further characterization is discussed below.

3.1 Methodology

- **Sample preparation**

The samples were prepared by thermo-chemical reaction route. Their details are given below:

Attempts were made to synthesize chromium carbide nano-crystals via a simple thermo chemical reaction in a sealed autoclave using organic solvent (acetone) and chromium oxide under the autogenic pressure in presence of reducing element, Mg at the temperature ranging from 600-800^oC.

The possible reaction at high temperature and pressure can be formulated as follows:

$$3Cr_2O_3 + 2C_3H_6O + 10Mg \rightarrow 2Cr_3C_2 + 10MgO + C + CO\uparrow + 6H_2\uparrow$$

Synthesis of chromium carbide nanoparticles

Experiments were conducted in a specially designed autoclave of 40 ml capacity. In this experiment, effect of reaction time has been studied with variation in temperature at 600^oC, 700^oC and 800^oC. The experimental procedure followed is shown in fig. 3.1. However, the details of ingredients taken for each experiment are given in tabular form in next section for simplicity and also to analyse the results properly.

Experimental Frame-Work

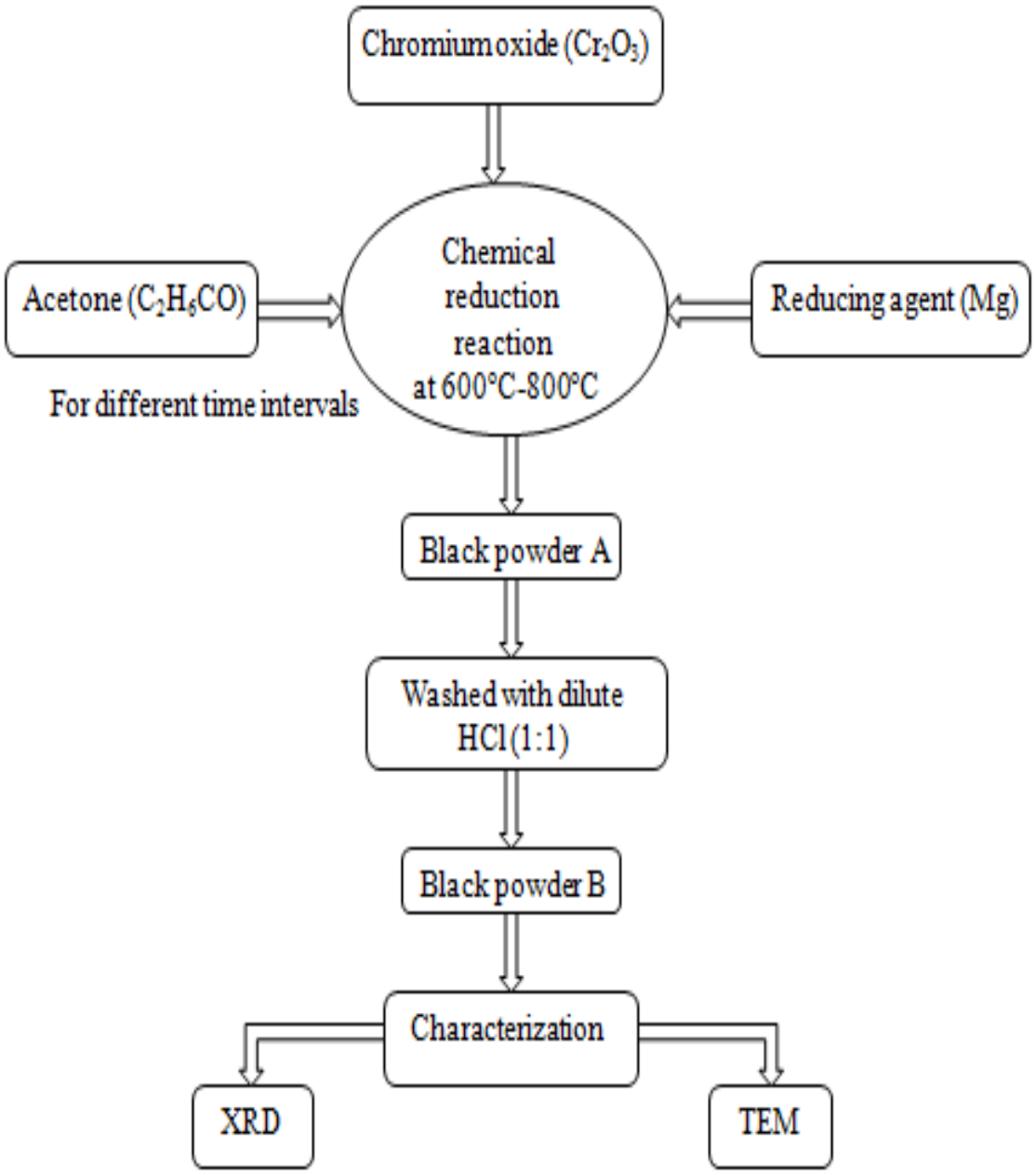

Fig. 3.1 Schematic representation of experimental procedure.

The initial ingredients chromium oxide (Cr_2O_3), magnesium turnings and a hydrocarbon (acetone) as a carbon source were put in the autoclave. After proper sealing, the autoclave was heated up to a desired temperature (i.e., 600^{o}C, 700^{o}C and 800^{o}C), held at that temperature for a certain time period (i.e., 5h, 10h, 15h, and 20h) and cooled down to room temperature in the furnace. The black powder of the reaction product thus obtained was removed. The reaction product was further leached by dilute HCl (1:1) to remove the by-products of the reaction product to get chromium carbide phase.

3.2 Characterization techniques

Characterization is an integral part of the study of the synthesized nano particles. The analysis of the synthesized nano powder samples was done by sophisticated techniques like X-ray diffraction (XRD) and transmission electron microscope (TEM). The details of these techniques are given below:

3.2.1 X-ray diffraction (XRD)

As prepared samples were characterized by X-ray diffractometer with CuK_α radiation for the identification of existing phases and their volume fractions, crystal structure, lattice parameter of the crystalline solids. i.e. how the atoms pack together in the crystalline state and what is the interatomic distance and angle. The sample is irradiated with monochromatic X-rays and the counters record the reflected radiation. The X-ray diffraction patterns were recorded using Bruker's diffractogram with CuK_α radiation (λ = 1.5418 Å) obtained from copper target using an in built Ni filter.

The interplanar spacing (d) of samples was calculated using the Bragg's law. The XRD patterns were identified using Powder Diffraction Files (PDF). The 2θ values for XRD patterns, in the range of 10^o to 90^o are sufficient to cover the most useful part of the powder pattern. Some peaks

in the XRD pattern were manually analyzed by comparing measured 2θ values (and d-spacings) with information on the relevant ICDD (The International Center for Diffraction Data) cards.

Crystallite size estimation

Based on the XRD technique, Debye and Scherer developed an equation to calculate crystal size from the broadening of a diffraction line at half the line maximum intensity by employing only ordinary principle of optical diffraction. The crystallite size was calculated by the following Debye-Sherrer equation:

$$\mathbf{r = 0.9\,\lambda / B\cos\theta_B} \qquad (1)$$

Where, r represents the crystallite size (Å), λ is the wavelength of X-rays (1.54 Å), B is the line width at half maxima (in radian) and θ_B is the angle of diffraction peaks (degrees). The accurate line broadening has been estimated by the following equation:

$$\mathbf{\Theta_{corr} = (\theta_o^2 - \theta_i^2)^{1/2}} \qquad (2)$$

Where, Θ_{corr} is the corrected value of the line broadening due to particle size, θ_o is the observed crystallite size of the powder samples.

3.2.2 Transmission electron microscopy (TEM)

Transmission electron microscopy (TEM) is used to obtain information from samples that are thin enough to transmit electron. TEM is almost always the first method used to determine the size and size distribution of nanoparticle samples. In TEM, the whole area of observation is illuminated using an electron source of adequate intensity. The transmitted electrons are generally used to form either an image or a diffraction pattern of the specimen. When a crystal of lattice spacing 'd' is illuminated with electrons of wavelength 'λ', the diffracted waves are produced at specific angles 2θ for n = 1, satisfying the Bragg's condition as:

$$\mathbf{2d \sin\theta = n\lambda}$$

The diffracted waves form diffraction spots on the back focal plane. In an electron microscope, the use of electron lenses allows the regular arrangement of diffraction spots to be projected on a screen and the electron diffraction pattern is observed. If the transmitted and the diffracted beam interfere on the image plane, a magnified image can be observed. The space where the diffraction pattern forms is called the reciprocal space, while the space at the image plane or at a specimen is called the real space. Samples are prepared for imaging by drying nanoparticles on a copper grid that is coated with a thin layer of carbon. Materials with electron densities that are significantly higher than amorphous carbon are easily imaged. The observational dimension selected from the object is usually limited to about 0.1 micrometer in diameter. However, in micro diffraction method, the diffraction pattern is obtained from an area correspondingly to only a few nanometres in diameter.

Sample preparation for TEM

For TEM study, the synthesized samples were first suspended in ethanol and sonicated for 15 minutes to obtain the uniform dispersion of nanoparticles. After sonication, one drop of suspension was dropped on carbon-coated copper grid and ethanol was allowed to evaporate before placing in a collecting container.

CHAPTER 4

RESULTS AND DISCUSSION

In the present study, experiments were performed to optimize the conditions to synthesize chromium carbide (Cr_3C_2) phase by varying the reaction time for a particular temperature. The approach to select the materials ratio is based on our earlier reports on the synthesis of WC, V_8C_7 phase using similar technique [54, 63].

Initial ingredients, their weights with sample label at varying temperature 600^{o}C, 700^{o}C, and 800^{o}C are compiled in the tables given below:

Table 4.1 Initial ingredients, their weights for the sample series (S_1-S_4) at temperature 600^{o}C.

Sample's label	Cr_2O_3 (gm)	Mg (gm)	Acetone (ml)	Reaction time (in hr)
S_1	1.5	3	25	5
S_2	1.5	3	25	10
S_3	1.5	3	25	15
S_4	1.5	3	25	20

Table 4.2 Initial ingredients, their weights for the sample series (S_5-S_8) at temperature 700^{o}C.

Sample's label	Cr_2O_3 (gm)	Mg (gm)	Acetone (ml)	Reaction time (in hr)
S_5	1.5	3	25	5
S_6	1.5	3	25	10
S_7	1.5	3	25	15
S_8	1.5	3	25	20

Table 4.3 Initial ingredients, their weights for the sample series (S_9-S_{12}) at temperature 800^{o}C.

Sample's label	Cr_2O_3 (gm)	Mg (gm)	Acetone (ml)	Reaction time (in hr)
S_9	1.5	3	25	5
S_{10}	1.5	3	25	10
S_{11}	1.5	3	25	15
S_{12}	1.5	3	25	20

4.1 X-ray diffraction analysis

The X-ray diffraction analysis of the prepared samples has been done in three domains of temperature i.e. at (1) 600^{o}C, (2) 700^{o}C and (3) 800^{o}C to analyze the influence of reaction time at constant composition of ingredients. The XRD pattern of these samples after acid treatment is shown in fig. 4.1 to 4.3. It shows the diffraction peaks of two main phases corresponding to

Cr_3C_2 (ICDD card no. 01-071-2287) with orthorhombic crystal structure and Cr_2O_3 (ICDD card no. 00-038-1479) with rhombohedral crystal structure. However, apart from this, broad peak ranging from 25^o to 28^o is also observed in all samples which correspond to nano carbon.

4.1.1 Influence of reaction time at 600°C

The XRD pattern of powders synthesized at 600°C for various reaction times is shown in fig. 4.1.

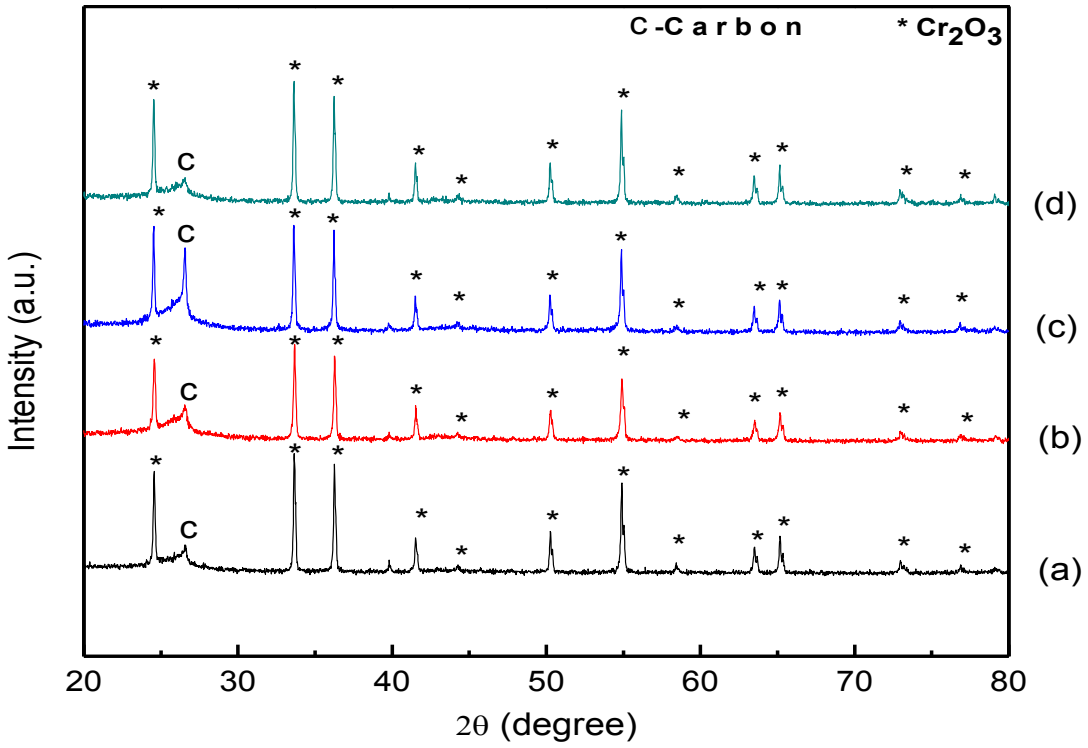

Fig. 4.1 X-ray diffraction pattern of the samples obtained at 600°C for (a) 5h, (b) 10h, (c) 15h and (d) 20h.

At reaction temperature of 600°C, XRD pattern displays sharp peaks, indexed with Cr_2O_3 phase. No peak of Cr_3C_2 phase has been observed which clearly indicate that the reaction temperature is not sufficient enough to reduce the chromium oxide. Broad peak of carbon indicates that at the temperature of 600°C, only pyrolytic decomposition of acetone has taken place which generates

carbon and other gases as shown in equation 1. The effect of these gases is discussed in the transformation kinetics of chromium oxide which is discussed later.

$$CH_3COCH_3 \rightarrow 2C + CO\,(g) + 6H_2\,(g) \qquad (1)$$

4.1.2 Influence of reaction time at 700°C

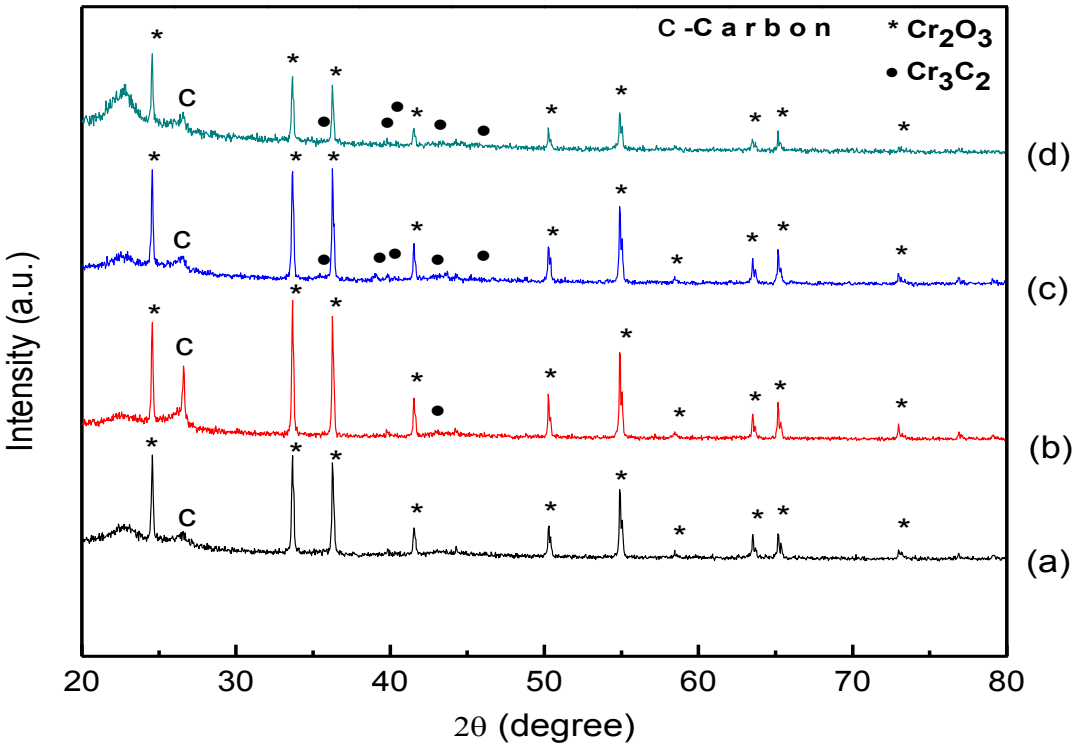

Fig. 4.2 X-ray diffraction pattern of the samples obtained at 700°C for (a) 5h, (b) 10h, (c) 15h and (d) 20h.

Heating the reaction mixture at 600°C could not lead to formation of chromium carbide phase. In order to get chromium carbide phase, the reaction temperature was increased to 700°C. The XRD pattern of product phase synthesized at 700°C is shown in fig. 4.2. It indicates that low reaction time even at 700°C as in case of samples S_5 and S_6 (5 and 10 h) does not provide sufficient time for diffusion of carbon in the matrix of chromium oxide for the formation of Cr_3C_2 phase. However, diffusion of carbon in chromium has been initiated at 700°C. As the time is increased

to 15 h in sample S_7 (fig. 4.2 (c)), some new peaks of Cr_3C_2 along with the Cr_2O_3 phase is observed. With increasing time to 20 h, the peak intensity of Cr_2O_3 phase decreases that shows the reduction process of chromium oxide (Cr_2O_3) to chromium carbide (Cr_3C_2) is being facilitated. It also confirmed from the volume fraction of the obtained phases as shown in table 4.4. With more holding time, volume fraction of chromium carbide increases with corresponding decrease in volume fraction of chromium oxide. The particle size calculated from Scherrer's formula does not show much variation in all the samples.

4.1.3 Influence of reaction time at 800°C

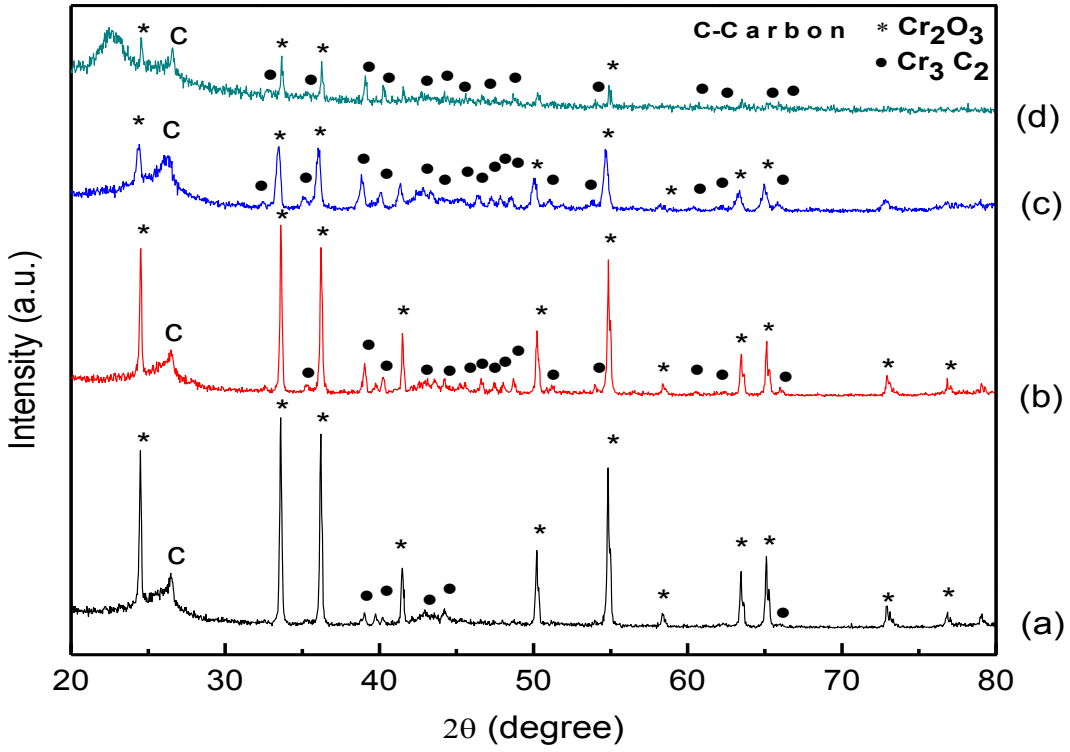

Fig. 4.3 X-ray diffraction pattern of the samples obtained at 800°C for (a) 5h, (b) 10h, (c) 15h and (d) 20h.

As temperature was further increased to 800°C, some more peaks of Cr_3C_2 phase of relatively

high intensity are observed. The XRD pattern of the synthesized product at 800^{o}C is shown in fig. 4.3. Again with more holding time, volume fraction of Cr_3C_2 has increased from 22 to 32% with corresponding decrease in the volume ratio of chromium oxide from 50 to 36% as shown in table 4.5. Also the broad hump in X-ray pattern for reaction time 15 h shows that the free carbon converted into amorphous phase.

Table 4.4 Crystallite size and volume fraction of samples synthesized at 700^{o}C.

Sample's label	Crystallite size	Volume fraction (%)		
	(in nm)	Carbide	Oxide	Carbon
S_5	36	21.2	50.1	28.6
S_6	38	27.2	48.4	24.4
S_7	30	31.1	48.7	20.1
S_8	35	31.1	36.4	32.3

Table 4.5 Crystallite size and volume fraction of samples synthesized at 800^{o}C.

Sample's label	Crystallite size	Volume fraction (%)		
	(in nm)	Carbide	Oxide	Carbon
S_9	40	22.4	51.0	26.0
S_{10}	24	30.3	40.5	28.6
S_{11}	42	32.2	34.1	33.6
S_{12}	63	32.1	34.1	33.8

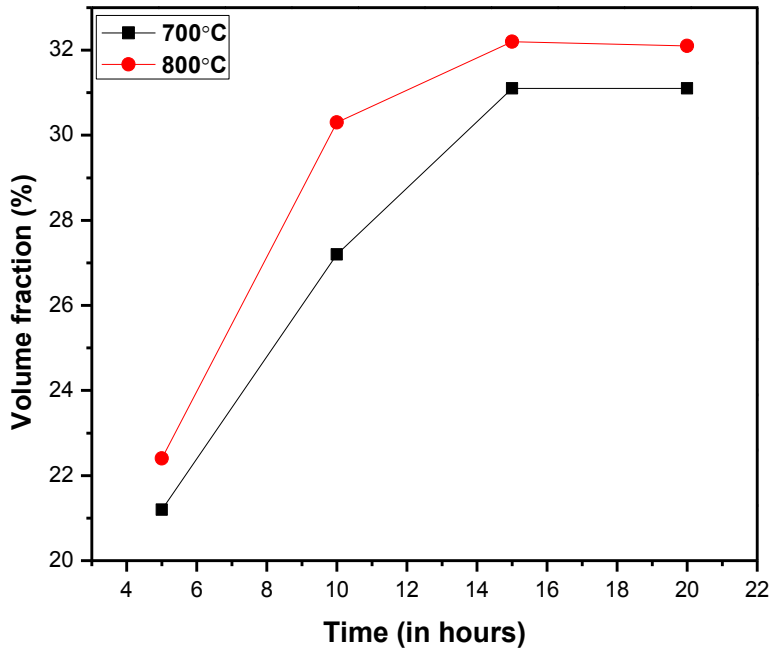

Fig. 4.4 Graph showing the variation between volume fractions of chromium carbide at varying time with increase in temperature.

Fig. 4.4 shows the graph between volume fractions of chromium carbide with variation in temperature at constant holding time. From the above graph, it is concluded that at same holding time, volume fraction of chromium carbide increases at 800^{o}C. Also at 800^{o}C, holding time of 15 h give rise to more fraction of chromium carbide as compared to 20 h, though the increment is not much but trend indicates that increasing the holding time further beyond 20 h may facilitate more amount of conversion of Cr_2O_3 to Cr_3C_2 phase. In order to get it further experiment is being carried out.

4.2 TEM analysis

Our X-ray analysis indicate that samples prepared at 700^{o}C and 800^{o}C for higher holding time exhibit more volume fraction of Cr_3C_2 phase as compared to samples synthesized at low temperature with less holding time. Considering these facts, TEM analysis of samples synthesized at 700^{o}C and 800^{o}C has been done. Fig. 4.5 to 4.8 shows the TEM images of the synthesized samples. These images show the formation of different features obtained during carburization. TEM analysis shows that there exists free carbon in all the synthesized samples. Only the amount of carbon varies from one product to other.

In order to understand the transition of Cr_2O_3 to Cr_3C_2, it is necessary to understand the various processes that take place during heating and cooling of the autoclave. In all the reactions, Mg is added as reducing element, which takes oxygen from the reaction atmosphere and is converted into MgO, which act as an active catalyst for further reaction.

In the presence of base catalyst, decomposition of acetone occurs at 200-300^{o}C and generates carbon, carbon monoxide and hydrogen gases as given in eq. 1. Because of the presence of these gases, pressure inside the autoclave increases which helps in the reduction of Cr_2O_3 to chromium (Cr). The carbon thus generated during pyrolytic decomposition of acetone, is deposited on the surface of Cr_2O_3. In due course of time it migrates inside the lattice of Cr_2O_3 through the process of diffusion. The continuous deposition and diffusion of carbon reduces the Cr_2O_3 to Cr and from the Cr to form final product chromium carbide (Cr_3C_2). With time, more and more carbon gets deposited on the surface of the precursor to enhance the diffusion process. This process continues till the surface gets saturated with carbon and ultimately forms chromium carbide (Cr_3C_2).

The chemical reactions proposed in this process could be formulated as follows:

$$CH_3COCH_3 \rightarrow 2C + CO\ (g) + 6H_2\ (g)$$

$$Cr_2O_3 + 3Mg \rightarrow 2Cr + 3MgO$$

$$3Cr + 2C \rightarrow Cr_3C_2$$

Since the growth of carbides occurs as faceted type to have high stability as predicted by Jackson and Hunt model [66, 67] so the smaller particles having very small size get aligned as shown in fig. 4.5 (a) and acquire large facets structure as shown in fig. 4.5 (b and c). The microstructures showing large facets obtained from various reactions are shown in fig. 4.5 to 4.8.

After the diffusion, carbon continues to get deposit on the surface leading to the formation of solid carbon spheres as shown in fig 4.5 (d). Consequently, these carbon nanospheres (CNS) encapsulate the carbide nanoparticles which are shown by dark inner zone in fig. 4.5 (e) and 4.6 (b). Moreover, broad peak of carbon in XRD pattern also shows the core-shell nanocomposite of Cr_3C_2-C with time, these spheres forms a loop around which interwoven type structure can be seen as shown in fig. 4.5 (f) which with time is converted into carbon nanotubes [54].

From TEM analysis of all the samples, it is concluded that less holding time leads to the formation of carbon spheres with less volume fraction of chromium carbide (Cr_3C_2) whereas no such structures can be seen in higher holding time as shown in fig 4.8 in which more fraction of Cr_3C_2 is obtained. These results are also in good agreement with our XRD results. Diffraction pattern recorded from the selected area also shows the presence of Cr_3C_2 and Cr_2O_3 phases both as shown in Fig. 4.9 (b), 4.10 (b).

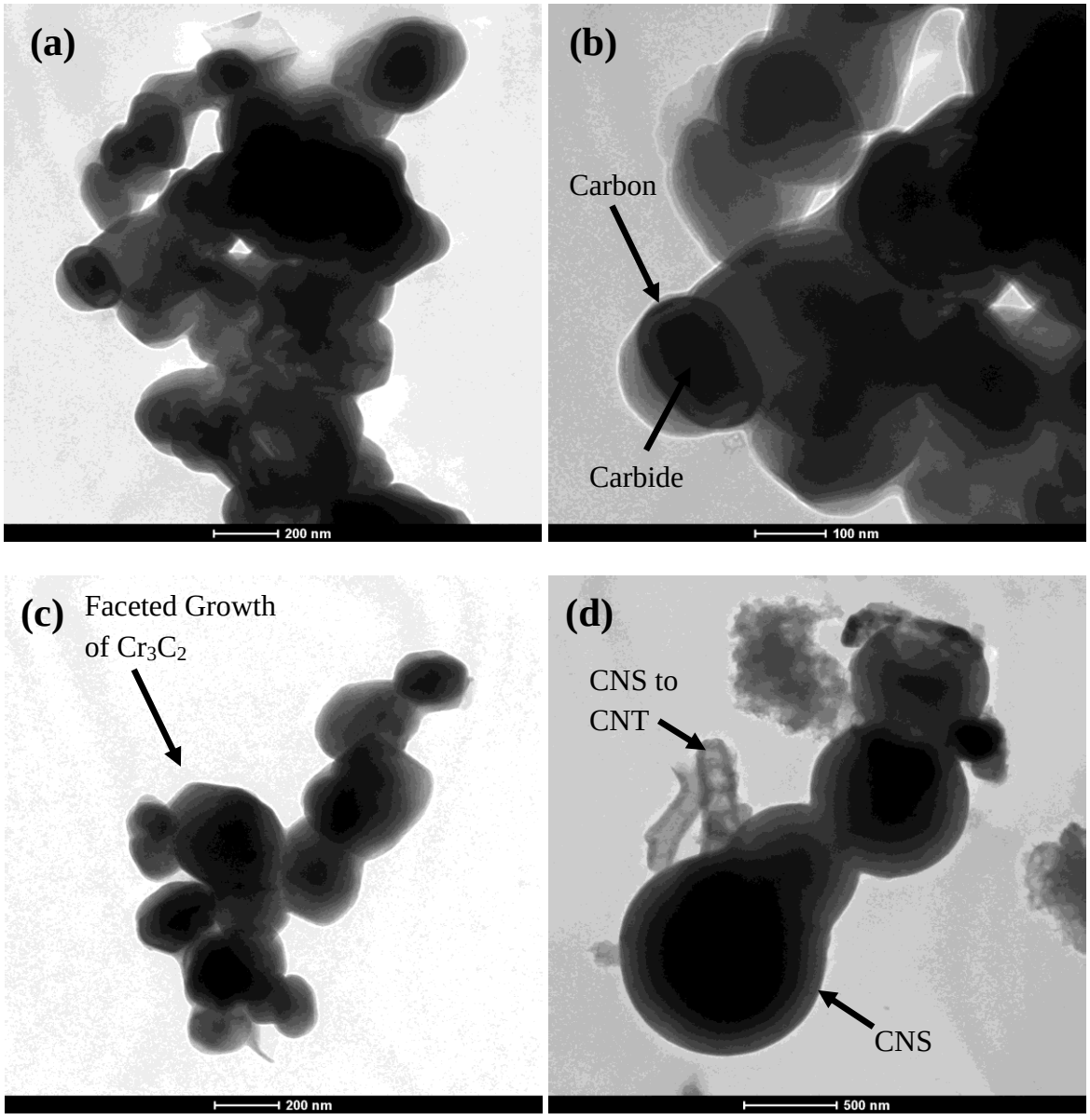
(a)
200 nm
(b)
Carbon
Carbide
100 nm
(c)
Faceted Growth
of Cr_3C_2
200 nm
(d)
CNS to
CNT
CNS
500 nm

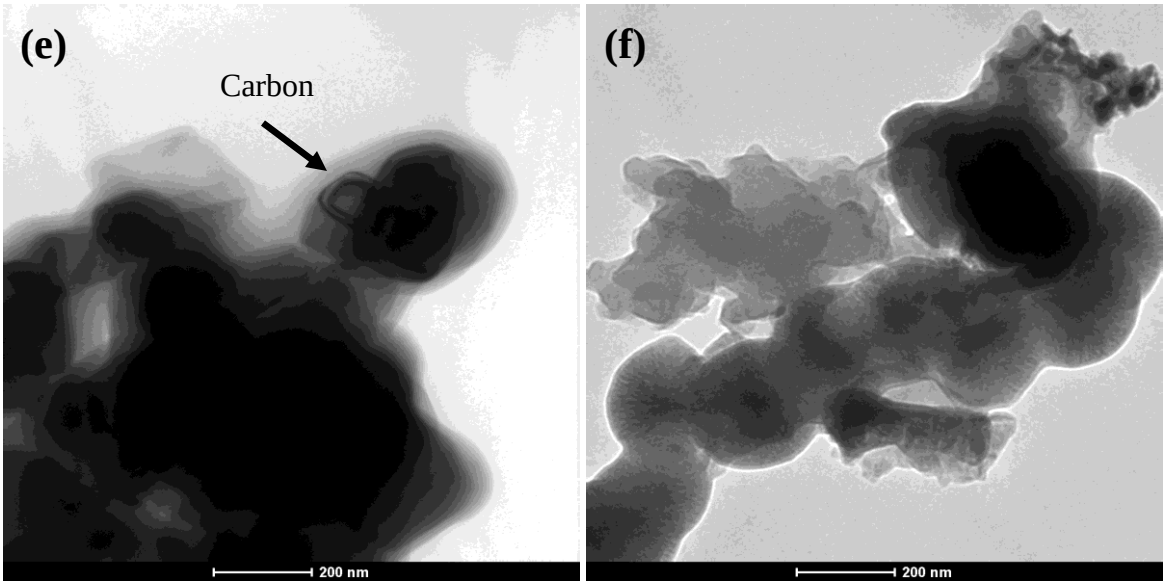

Fig. 4.5 TEM micrographs of the sample S_7.

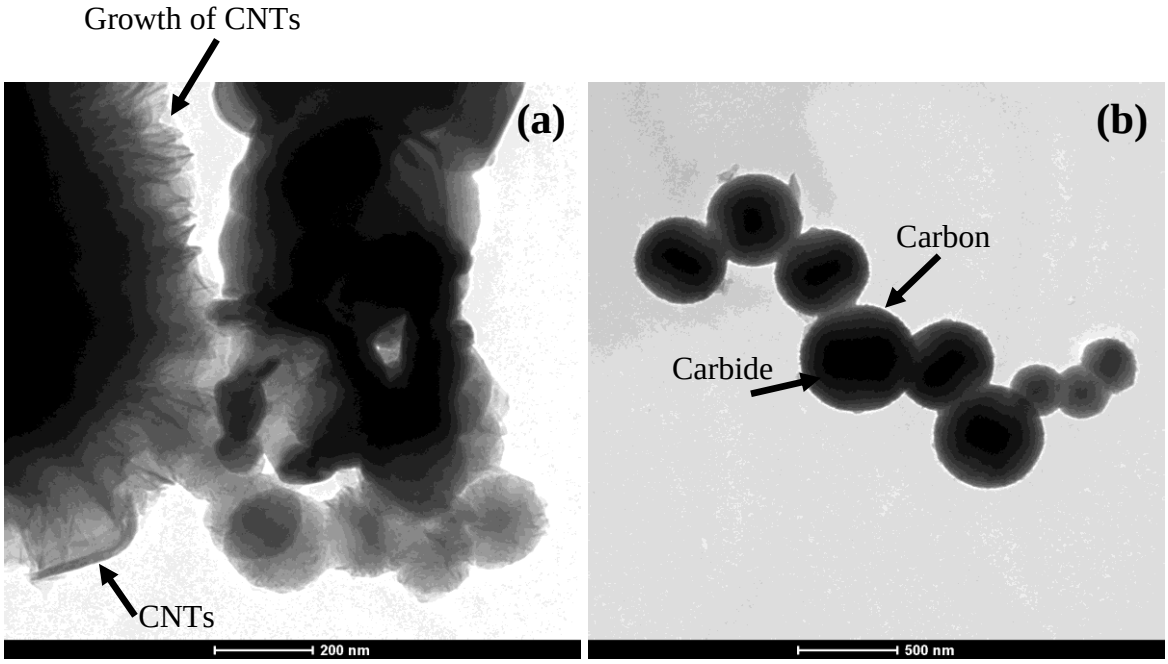

Fig. 4.6 TEM micrographs of the sample S_8.

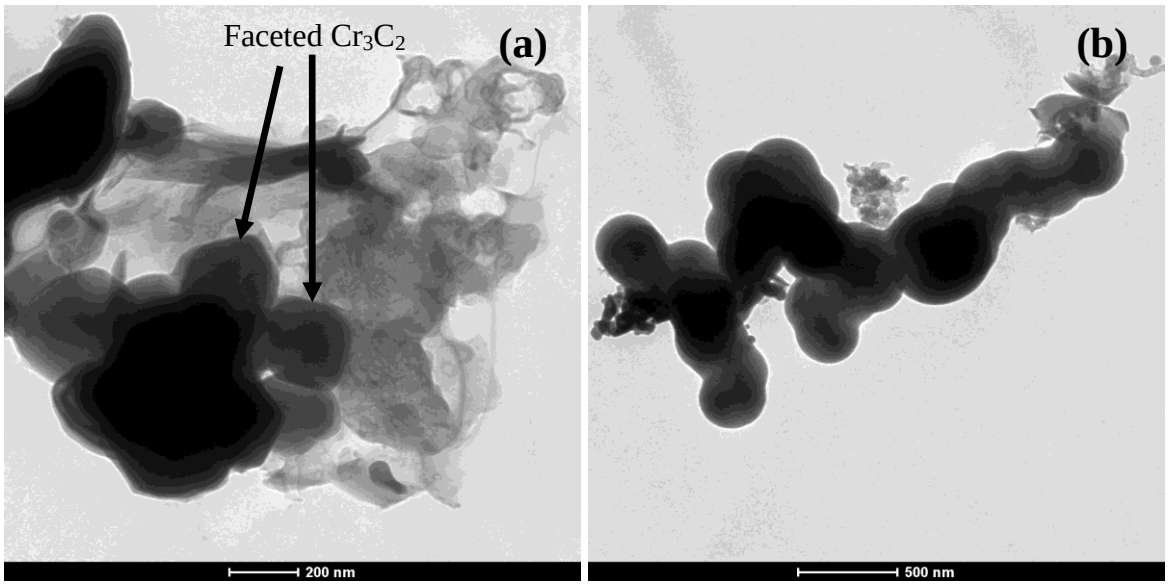

Fig. 4.7 TEM micrographs of the sample S_{11}.

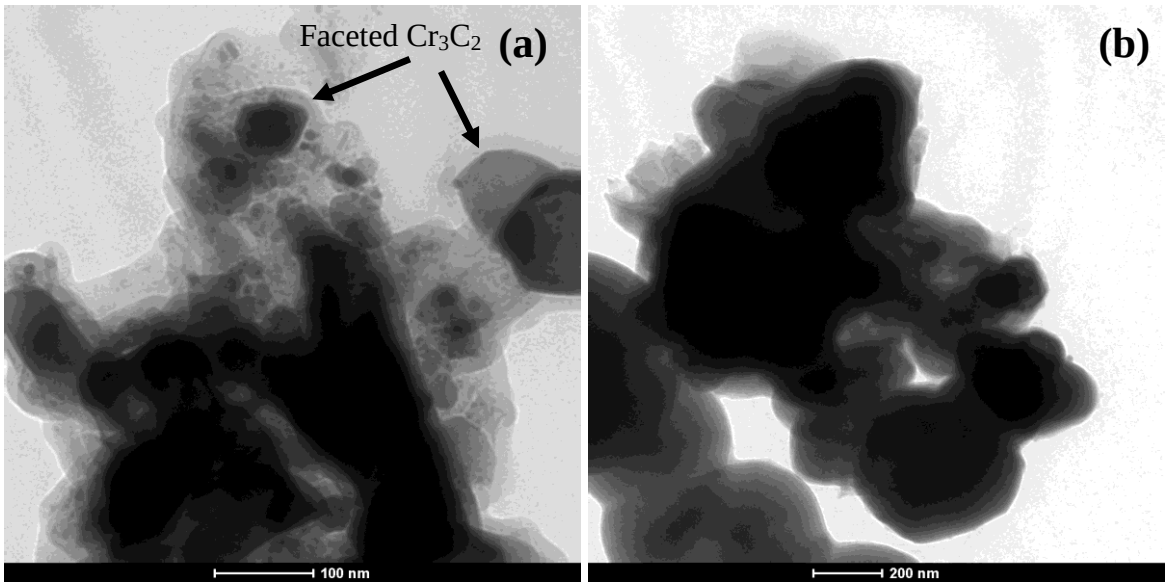

Fig. 4.8 TEM micrographs of the sample S_{12}.

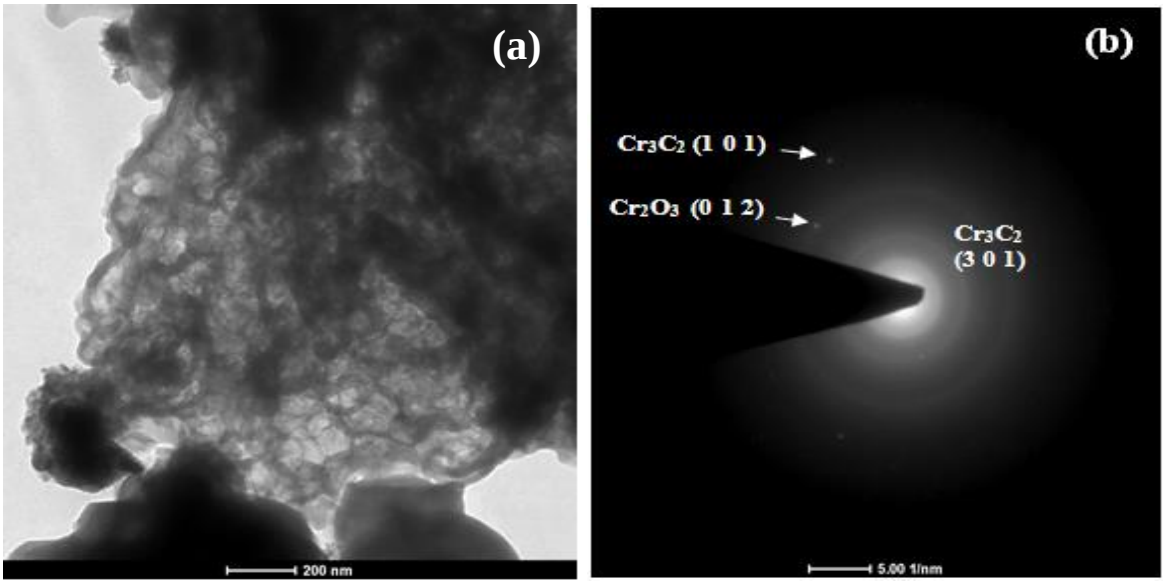

Fig. 4.9 TEM micrograph of sample S_{11} showing the presence of different features, (b) corresponding diffraction pattern taken from particles showing the planes of (101) and (301) for the Cr_3C_2 phase.

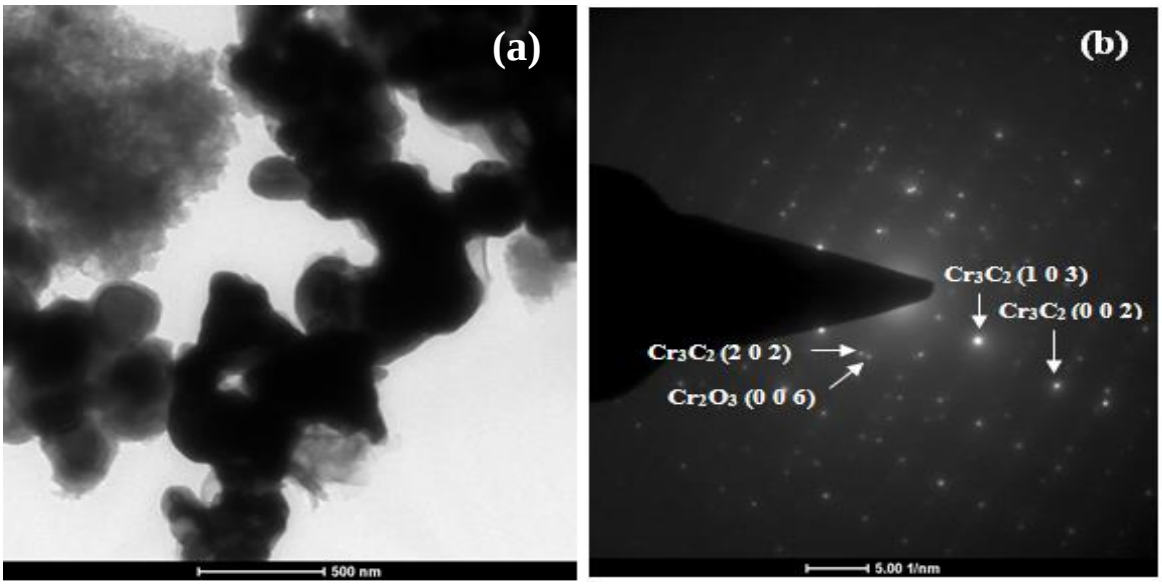

Fig. 4.10 TEM micrograph of sample S_{11} showing the presence of different features, (b) corresponding diffraction pattern taken from particles showing the planes of (202), (103) and (002) for the Cr_3C_2 phase.

The EDS spectra shown in fig. 4.11 also shows the presence of carbon and chromium as major phases in the product, which further confirms with the obtained XRD results.

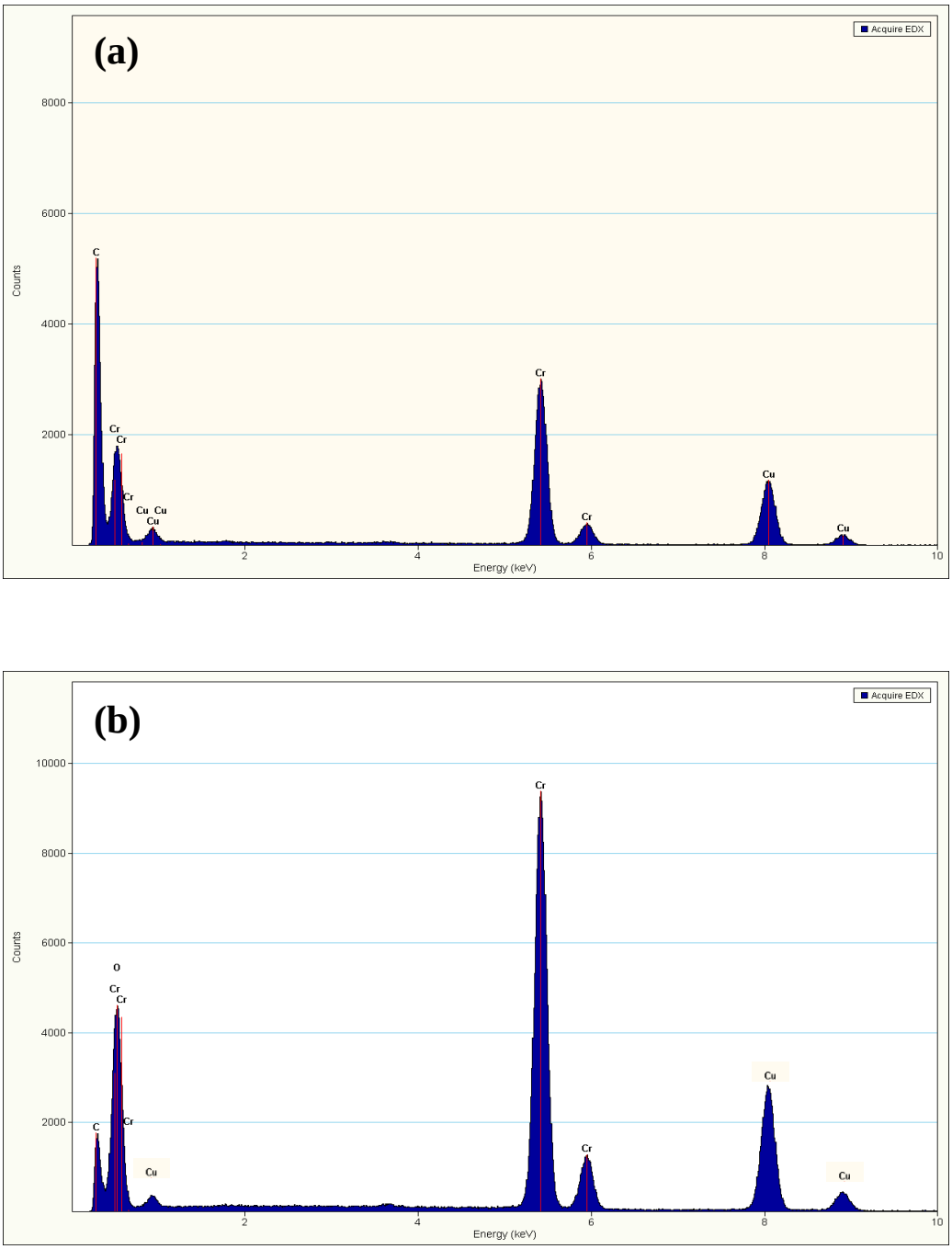

Fig. 4.11 EDS spectra showing the presence of Cr and carbon phases of the sample (a) S_7 & (b) S_{11}.

CHAPTER 5

CONCLUSIONS & FUTURE SCOPE

The present study indicates that chromium carbide (Cr_3C_2) nanopowder can be synthesized by chemical-reaction route under high pressure. Since no reports of such study exist in literature so it can be considered as major breakthrough. However, complete transformation of Cr_2O_3 to Cr_3C_2 is not obtained but it shows the feasibility to get it by optimizing the processing conditions. Based on the experimental results, transformation kinetics from reactant to resultant product has been studied. From TEM analysis it is concluded that the synthesized nano particles has faceted morphology. Also formation of carbon spheres during reduction has been observed. This route has the potential to synthesize the pure product but requires further optimization.

The results of present investigation indicate that complete reduction of Cr_2O_3 did not take place and we find the presence of Cr_3C_2 phase along with Cr_2O_3 and carbon as impurity in the final product. But high fraction of Cr_3C_2 at 800^oC shows the possibility of formation of single phase nano chromium carbide powder with optimized processing parameters.

By considering all these facts, it is observed that optimized condition to obtain pure Cr_3C_2 has to be established. Further, more reactions with different carbon sources should be carried out to get good yield and better quality of the final product. Suitability of as-synthesized powders can be checked in WC-Co as grain growth inhibitor. Catalytic activities of chromium carbide can also be checked for solid-oxide fuel cells (SOFCs) and also in proton exchange membrane fuel cells (PEMFCs).

REFERENCES

1) R. Edwards, “Cutting Tools’’, The Institute of Materials, London, (1993).
2) E. M. Trent, “Metal Cutting”, Butterworths, Boston, 2nd Ed., (1984).
3) Z. Yan, H. Meng, P. K. Shen, R. Wang, L. Wang, K. Shi, H, Fu, J. Mater. Chem., 22, 5072, (2012).
4) H. O. Pierson, Handbook of Refractory Carbide and Nitride, 16, (1996).
5) M. R. Wehr, J. A. Richards, T. W., Jr. Adair, III, Physics of the Atom, Addison-Wesley Publishing Co., Reading, MA, (1978).
6) R. C. Evans, An Introduction to Crystal Chemistry, Cambridge Univ. Press, Cambridge, (1979).
7) L. E. Toth, Transition Metal Carbides and Nitrides, Academic Press, New York, (1971).
8) S. T. Oyama, J. Solid State Chem., 96, 442, (1992).
9) H. Tulhoff, Carbides, in Ullmann S Encyclopedia of Industrial Chemistry, 5^{th}. Ed., Vol. 15, VCH (1985).
10) R. E. Rundle, Acta Cryst, 1, 180, (1948).
11) R. B. Levy, M. Boudart, Science, 181, 547, (1983).
12) H. J. Goldschmidt, Interstitial Alloys, Butterworth, Washington, DC, (1967).
13) B. E. Douglas, D. H. Mac Daniel, Concepts and Models of Inorganic Chemistry, Wiley, New York, (1965).
14) D. Y. Wang, K. W. Weng, C. L. Chang, W. Y. Ho., Surf. Coat. Technol., 120, 622, (1999).

15) J. M. Guilemany, J. M. Miguel, S. Vizcaino, C. Lorenzana, J. Delgado, J. Sanchez, Surf. Coat. Technol., 157, (2002).

16) J. L. Vossen, W. Kern, In Thin Film Processes; Academic Press, New York, (1978).

17) K. Klabunde, Y. X. Li, B. J. Tan, Chem. Mater., 3, 39, (1991).

18) R. E. Kahrizsangi, H. M. Zadeh, V. Nemati, Int. J. Ref. Met. Hard Mater., 28, 415, (2010).

19) C. J. Brinker, G. W. Scherer, Sol-Gel Science, The Physics and Chemistry of Sol-Gel Processing; Academic Press: New York, (1990).

20) Z. Zhao, H. Zheng, Y. Wang, S. Mao, J. Niu, Y. Chen, M. Shang, Int. J. Ref. Met. Hard Mater., 29, 617, (2011).

21) O. M. Cintho, E. A. P. Favilla, J. Alloys Compd., 439, 195, (2007).

22) P. Schwarzkopf, R. Kieffer, W. Leszynski, F. Benesovsky, Refractory hard metals: borides, carbides, nitrides and silicides, New York, (1953).

23) C. T. Fu, A. K. Li, C. P. Lai, J. R. Duann, High performance ceramic composites containing tungsten carbide reinforced chromium carbide matrix, US Patent No. 5580833, (1994).

24) "Advances in Nanocomposite Technology", edited by Abbas Hashim, DOI: 10.5772/17899, July 27, (2011).

25) K. Juhani, J. Pirso, M. Viljus, S. Letunovits, M. Tarraste, Materials Science (Medziagotyra), 18, 83, (2012).

26) S. Luyckx, M. Z. Alli, Mater. & Design 510, 22, (2001).

27) R. Dagani, "Nanostructured Materials Promise to Advance Range of Technologies", Chemical & Engineering News, Nov. 23, 24, (1992).

28) K. Schrter, US Patent 1, 549, 615 (application Oct. 31, 1923; patented 1925).

29) P. Schwarzkopf, Deutsche Edelstahlwerke, AG German Patent 720, 502 (patented 1929, issued 1942).

30) R. A. Paris, E. Clar, Angewandte Chemie-International Edition, 75, 725, (1963).

31) D. Thihaudon, M. Rcuhin, R. A. Paris, J. Paris, Planseeber Pulvermetall, 20, 129, (1972).

32) H. E. Exner and J. Gurland, Powder Metallurgy Int., Vol. 2, 2, (1970).

33) P. Craig, "Behind the Carbide Curtain", Cutting Tool Engineering, 26, (1997).

34) E. Ivanov, G. Golubkova, J. Alloys Compd., 190, (1992).

35) A. Lerch, A. Rousset, Thermochim. Acta, 232, 233, (1994).

36) S. Loubiere, Ch. Laurent, J. P. Bonino, A. Rousset, Mater. Res. Bull., 30, 1535, (1995).

37) S. Loubiere, Ch. Laurent, J. P. Bonino, A. Rousset, J. Alloys. Compd., 243, 59, (1996).

38) K. C. Walter, J.T. Scheuer, P.C. McIntyre, P. Kodali, N. Yu, M. Nastasi, Surf. Coat. Tech., 85, 6, (1996).

39) S. Hashimoto, A. Yamaguchi, J. Am. Ceram. Soc., 79, 2503, (1996).

40) S. K. Ko, C. W. Won, I. J. Shon, Scripta Mater., 37, 889, (1997).

41) M. Detroye, F. Reniers, C. Buess-Herman, J. Vereecken, App. Surf. Science, 120, 85, (1997).

42) H. Preiss, D. Schultze and K. Szulzewsky, J. Eur. Ceram. Soc., 19, 187, (1998).

43) J. He, M. Ice, and E J. Lavernia, Nano Struct. Mater., 10, 1283, (1998).

44) D. E. Wolfe, J. Singh, K. Narasimhan, Surf. Coat. Tech., 160, 218, (2002).

45) J. Romero, A. Lousa, E. Martinez, J. Esteve, Surf. Coat. Tech., 163, 392, (2003).

46) Y. L. Su, T. H. Liu, C. T. Su, J. P. Yur, W. H. Kao, S. H. Yao, J. Mater. Pro. Tech., 153, 699, (2004).

47) N. Anacleto, O. Ostrovski, Metall. Mater. Trans. B, Vol 35B, 612, (2004).

48) L. D. Teng, X. G. Lu, R. E. Aune, and S. Seetharaman, Metall. Mater. Trans. A, Vol 35A, 3680, (2004).

49) S. Sen, Vacuum, 79, 63, (2005).

50) H. T. Lin, W. S. Huanga, S. C. Wang, H. H. Lu, W. Cheng, J. Wei, J. L. Huanga, Mater. Sc. and Engg. B, 127, 28, (2006).

51) C. C. Lin, W. J. Hsieh, J. H. Lin, U. S. Chen, X. J. Guo, H. C. Shih, Surf. Coat. Tech., 200, 5052, (2006).

52) O. M. Cintho, E. A. P. Favilla, J. Alloys Compd, 439, 189, (2007).

53) C. Giordano, C. Erpen, W. Yao, B. Milke, and M. Antonietti, Chem. Mater., 21, 5144, (2009).

54) A. Kumar, K. Singh, O. P. Pandey, Physica E, 41, 684 (2009).

55) S. C. Wang, H. T. Lin, P. K. Nayak, S. Y. Chang, J. L. Huang, Thin Solid Films, 518, 7360, (2010).

56) R. Ebrahimi K., H. M. Zadeh, V. Nemati, Int. J. Ref. Metal. Hard Mater., 28, 415, (2010).

57) S. Gomari, S. Sharafi, Journal of Alloys Compd., 490, 30, (2010).

58) T. Xing, X. Cui, W. Chen, R. Yang, Mater. Chem. Phy., 128, 181, (2011).

59) Z. Zhao, H. Zheng, Y. Wang, S. Mao, J. Niu, Y. Chen, M. Shang, Int. J. Ref. Metal. Hard Mater., 29, 614, (2011).

60) M. W. Richert, M. Ksiazek, P. Palka, S. Wawrzyniak, R. Grzelka, K. Plonska-Niznik, J. Ach. Mater. Manf. Engg, 55, (2012).

61) T. Jiang, I. O. Wallinder, G. Herting, ISRN Corrosion, 2012, 10, (2012).

62) L. Wang, Q. Li, Yongchun Zhu, Y. Qian, Int. J. Ref. Metal. Hard Mater., 31, 292, (2012).

63) M. Mahajan, K. Singh, O. P. Pandey, Int. J. Ref. Metal. Hard Mater., 36, 110, (2013).

64) C. Ouyang, S. Zhu, W. Dong, H. Qu, Int. J. Ref. Metal. Hard Mater., DOI 10.1016/j.ijrmhm.2013.01.015, (2013).

65) L. Zhang, K. Goa, A. Elias, Z. Dong, W. Chen, Ceram. Int., DOI 10.1016/j.cermint.2013.05.122, (2013).

66) K. A. Jackson, J.D. Hunt, Acta Metall., 13, 1212, (1965).

67) A. Ludwig, S. Leibbrandt, Mat. Sci. Eng. A, 540, 375, (2004).